Optics Letters

Spatial resolution enhancement of coherent Doppler wind lidar using differential correlation pair technique

Yunpeng Zhang,[1] Yunbin Wu,[1] and Haiyun Xia[1,2,3,4,*]

[1]School of Earth and Space Sciences, University of Science and Technology of China, Hefei 230026, China
[2]School of Atmospheric Physics, Nanjing University of Information Science and Technology, Nanjing 210044, China
[3]Hefei National Laboratory for Physical Sciences at the Microscale, USTC, Hefei 230026, China
[4]Institute of Software, Chinese Academy of Sciences, Beijing 100190, China
*Corresponding author: hsia@ustc.edu.cn

Received 3 September 2021; revised 10 October 2021; accepted 15 October 2021; posted 15 October 2021 (Doc. ID 442121); published 3 November 2021

A high spatial resolution coherent Doppler wind lidar (CDWL) incorporating the differential correlation pair (DCP) technique is proposed and demonstrated. By employing pulse pair with appropriate window functions, the spatial resolution can be enhanced, as the common parts of the correlation pair can be eliminated in the differential data processing. The performance of the new method is validated in the comparison experiment with the CDWLs adopting conventional schemes. Under a given peak power, the DCP technique provides higher wind velocity accuracy compared with a conventional pulsed CDWL where the laser spectral broadening caused by short pulses can be avoided and the carrier-to-noise ratio is improved. At a laser peak power of 250 W, with a spatial and temporal resolution of 3.3 m and 1 s, continuous radial wind profiling over 700 m is realized with a maximum error of 0.1 m/s.

https://doi.org/10.1364/OL.442121

Doppler wind lidar has been widely applied in scientific research and engineering applications, such as gravity waves observation [1,2], boundary layer evolution [3], weather forecast [4], air pollution monitoring [5,6], and wind energy exploitation [7]. Specifically, as a powerful remote sensing technique, CDWL provides spectrum information, which can be used for precipitation observation [8], cloud identification [9], and other applications. In fields like aviation safety and aerodynamics design, high spatial resolution wind detection is required [10,11].

In a typical pulsed CDWL system, the spatial resolution is determined by the pulse duration. To improve the spatial resolution, a straightforward way is shortening the pulse duration. But this simple approach will lead to two negative effects. First, as the pulse duration decreases, the spectral width of the backscatter signal increases. A broadened spectrum leads to the deterioration of the estimation accuracy of the wind velocity [12,13]. Second, the peak power of a fiber laser is usually limited by the nonlinear effects, especially with stimulated Brillouin scattering [14]. Under a limited peak power, the decrease of the pulse duration will lead to the reduction of the intensity of the atmospheric backscatter signal.

Despite all these difficulties, some CDWL systems with a spatial resolution less than 10 m have been proposed. In 2015, NASA proposed an all-fiber CDWL with configurable pulse durations from 50 to 400 ns, achieving a minimum spatial resolution of 7.5 m [15]. In 2019, a pulse-coding CDWL with 40 ns pulse duration was proposed by USTC, improving the spatial resolution to 6 m [16].

To further enhance the spatial resolution and wind velocity estimation accuracy, the disadvantages of short pulses need to be particularly addressed. Recently, as an approach to mitigate the short-pulse effects, some methods based on pulse pair were proposed in distributed fiber sensors [17–19]. In these methods, as the backscattering spectra are obtained from the difference of the backscatter signal's cross-correlation, the methods are named as the differential correlation pair (DCP) technique. In this Letter, a high-spatial-resolution CDWL utilizing DCP technique is demonstrated.

The system layout of the DCP lidar is shown in Fig. 1(a). A continuous-wave (CW) laser at 1550 nm is split into two parts. A minor portion of the CW laser is frequency shifted 80 MHz by an acousto–optic modulator (AOM), acting as the local oscillator (LO). The main portion of the CW laser serves as the seed of the transmitted signal. To modulate the continuous signal into pulses with designed shapes, cascaded electro-optic modulators (EOM) are employed to provide sufficient extinction ratio and modulation bandwidth. Different from the square pulses in [18], truncated Gaussian pulses are used here. Compared with square pulses, the generating Gaussian pulses are easier, especially in lidar systems where high-power erbium-doped fiber amplifiers (EDFA) are used. The no-light state is set at the truncated point of the Gaussian function to avoid the sudden change of laser power. During measurements, the two paired pulses will be transmitted by time division multiplexing with a sufficient time interval to avoid range aliasing. As illustrated in Fig. 1(b), the odd pulse in the pair is composed of a long common pulse

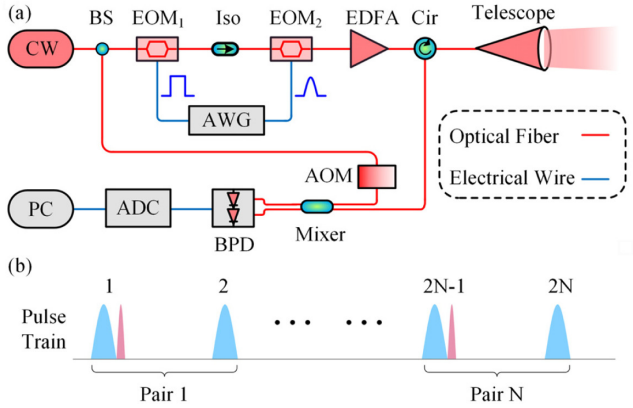

Fig. 1. (a) System layout of the DCP lidar. CW, continuous-wave laser; BS, beam splitter; Iso, isolator; AOM, acousto–optic modulator; EOM, electro-optic modulator; EDFA, erbium-doped fiber amplifier; Cir, circulator; BPD, balanced photodetector; ADC, analog-to-digital converter; AWG, arbitrary wave generator; and PC, personal computer. (b) Transmitted pulse train in the pair method.

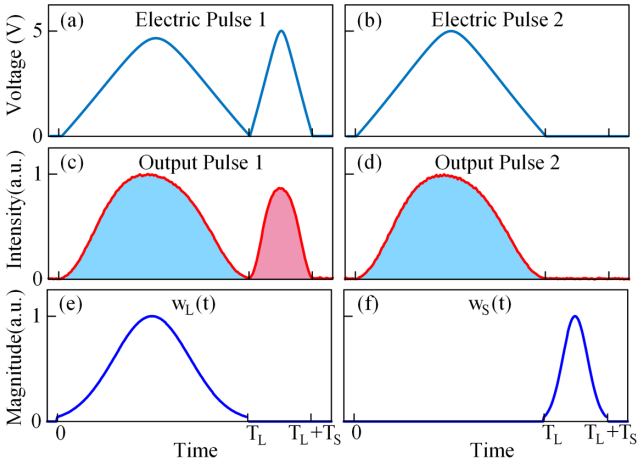

Fig. 2. (a) Modulating signals of the odd and (b) even pulse in the pair. (c) Measured laser waveforms of the odd and (d) even pulse. (e) The long and (f) short Gaussian window function used for data processing.

(cyan) and a short probing pulse (pink), while the even pulse only contains the common pulse.

The modulating signals fed to the EOM_2 are shown in Figs. 2(a) and 2(b), in which the sinusoidal transfer function of the EOM_2 has been considered. To facilitate shape forming, the pulses are truncated at $T_L = 300$ ns and $T_S = 100$ ns, respectively. Since the waveform could be distorted by the time-dependent gain profile in the EDFA [20], the output signal of the EOMs is carefully tailored to minimize the difference between the amplified common parts, and the relative difference less than 0.3% is achieved. Figures 2(c) and 2(d) show the measured waveforms of the amplified pulse pair in the experiment. The full-width at half-maximum (FWHM) pulse durations of the common pulse (τ_{pL}) and probing pulse (τ_{pS}) are configured to be 180 ns and 60 ns, respectively.

For the ith ($i = 1, 2$) pulse in the pair, the optical atmospheric backscatter signal will be collected by a 100-mm telescope and mixed with a LO. After beating on a balanced photodetector (BPD), the optical signal is converted into an intermediate frequency (IF) band electrical signal. Then the IF signal will be digitized by an analog-to-digital converter (ADC) and processed with the following algorithm, as depicted in Fig. 3.

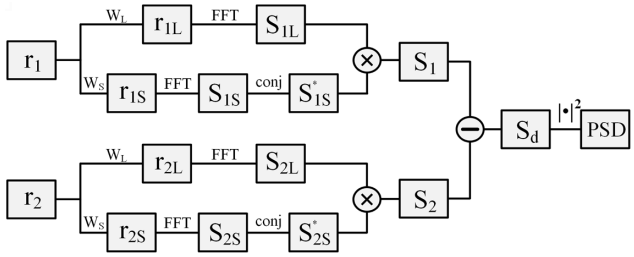

Fig. 3. Processing flow of the DCP lidar algorithm, where conj refers to the complex conjugate, and $|\cdot|^2$ refers to the square of modulus.

To retrieve the wind velocity at distance z_0, the digitized IF signal $r_i(t)$ is first windowed by functions $W_L(t - t_0)$ and $W_S(t - t_0)$ with $t_0 = 2z_0/c$. As shown in Figs. 2(e) and 2(f), the window functions are set to be Gaussian function with the same truncation length as the common pulse and probing pulse, respectively. We mark the windowed IF signal as $r_{iL}(t, z_0)$ and $r_{iS}(t, z_0)$, and their cross-correlation $R_i(\tau, z_0)$ is defined as [17]

$$R_i(\tau, z_0) = \int r_{iL}(t, z_0) r_{iS}(t + \tau, z_0) \mathrm{d}t. \tag{1}$$

The backscattering spectrum with enhanced spatial resolution can be obtained from the fast Fourier transform (FFT) of the differential cross-correlation

$$S_d(\nu, z_0) = \mathrm{FFT}_\tau \{R_1(\tau, z_0) - R_2(\tau, z_0)\}. \tag{2}$$

After accumulation, the power spectral density (PSD) of the differential cross-correlation can be finally expressed as

$$\mathrm{PSD}(\nu, z_0) = |\langle S_d(\nu, z_0)\rangle|^2, \tag{3}$$

where the operation $\langle\cdot\rangle$ refers to averaging over a number of laser shots. When a Gaussian pulse and corresponding window function are used, the spatial resolution is determined by both pulse duration and window function, specifically [21]

$$\Delta R = \frac{1}{2} c \left(\sqrt{\pi} \cdot \sqrt{\sigma_p^2 + \sigma_w^2}\right), \tag{4}$$

where $\sigma_p = \tau_P/(2\sqrt{\ln 2})$, $\sigma_w = \tau_w/(2\sqrt{2 \ln 2})$, with τ_p and τ_w being the FWHM of the pulse intensity and the Gaussian window function, respectively, and c is the speed of light. As detailed in [19], the PSD of the differential cross-correlation only contains information from a range cell determined by the probing pulse and corresponding window function. Thus, the spatial resolution of the DCP lidar can be calculated from the duration τ_{pS} of the probing pulse and the τ_{wS} of the short Gaussian window function $W_S(t)$.

Note that the Fourier transform of the cross-correlation can be realized by the cross spectrum, the spectrum of the differential cross-correlation $S_d(\nu, z_0)$ could be directly obtained by [18]

$$S_d(\nu, z_0) = S_{1L} S_{1S}^* - S_{2L} S_{2S}^*, \tag{5}$$

where S_{iL} and S_{iS} are the frequency domain signal corresponding to $r_{iL}(t, z_0)$ and $r_{iS}(t, z_0)$ obtained by the FFT, and the superscript * means taking the complex conjugate.

To validate the CDWL with the DCP technique, a comparison experiment is carried out. The measurement of the DCP lidar is based on the accumulation of the pairs of pulses, and conventional CDWLs accumulate the backscattering spectrum of each single pulse. Thus, the conventional CDWL would be called single pulse (SP) lidar for brevity. In the DCP lidar, the FWHM pulse duration τ_{pL} and τ_{pS} are set to be 180 ns and 60 ns, respectively, and the FWHM of the Gaussian windows τ_{wL} and τ_{wS} are 141 ns and 47 ns, respectively. The odd and even pulses in the pair are separated by 60 μs. Meanwhile, the SP methods with a pulse duration of 180 ns and 60 ns and the same Gaussian window function as the DCP method are implemented to verify the correctness and confirm the spatial resolution of the DCP lidar. The three systems will be referred to as DCP-60ns, SP-180ns and SP-60ns, according to the FWHM pulse duration. They share the same peak power and temporal resolution of 250 W and 1 s, respectively, and the pulse (for SP) and pair (for DCP) repetition rates are both 8.3 kHz.

Measurement results of lidars in DCP and SP methods are plotted in Fig. 4, where the black long-dash line, orange short-dash line, and blue line stand for SP-180ns, SP-60ns, and DCP-60ns, respectively. As shown in Fig. 4(a), the SP-180ns has the highest narrowband carrier-to-noise ratio (CNR_n) due to its lowest spatial resolution, and the CNR_n of SP-60ns is about 10 dB lower. Meanwhile, the DCP-60ns has much higher CNR_n than SP-60ns under the same spatial resolution. This can be interpreted as the backscatter signal of the probing pulse is coherently enhanced by the backscatter signal of the common pulse from the same range cell in the correlation operation, while the common parts of the pair cancel out in the difference operation [19].

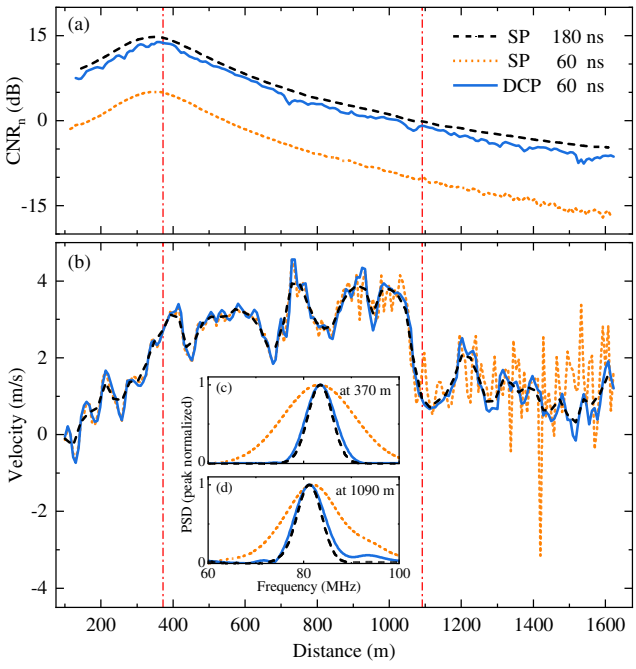

Fig. 4. (a) Narrowband CNR and (b) radial wind velocity profiles of the DCP lidar and SP lidars. Inset: normalized backscattering power spectrum density (PSD) at (c) 370 m and (d) 1090 m.

The backscattering power spectra at 370 and 1090 m are shown in Figs. 4(c) and 4(d) as insets. Due to the different data processing methods, the original PSD of the two schemes is scaled to different orders. For comparison, they are normalized by the peak value here. The FFT length is extend to 4096 through zero padding, corresponding to a sampling interval of 0.122 MHz in the frequency domain. In the two figures, the DCP-60ns and the SP-180ns have similar spectral width, while the spectrum of the SP-60ns is about three times wider. The narrow spectral width of the DCP-60ns can be easily explained by Fig. 3. The spectrum of signal r_i is greatly broadened by the short window function W_S but remains narrow under the long window function W_L. Thus, the product of a wide and a narrow spectrum limits the result to a narrow shape. As the wind velocity estimation is derived from the center frequency shift of the Gaussian fitting, a large spectral width would reduce the estimation accuracy [13]. For the blue line representing the spectrum from the DCP lidar, there are some sidelobes next to the narrow main peak, which mainly arise from the differential process. In theory, the common pulses of the pulse pair are designed to be the same. But in practice, despite careful control of the modulating signal feeding to the EOMs, distortion of the transmitted lasers cannot be avoided completely. Then the subtraction in Fig. 3 will lead to the sidelobes in the spectrum.

In Fig. 4(b), the radial wind velocity profile of the DCP-60ns is quite consistent with the SP-60ns within 800 m, confirming the DCP lidar's spatial resolution. Between 800 and 1600 m, the estimated wind velocity profile of the SP-60ns fluctuates noticeably, while that of the DCP-60ns can still follow the trend of the SP-180ns. This implies a better performance of the DCP method compared with the conventional SP method at the same laser peak power.

In a second experiment, the width parameter τ_{pS} and τ_{wS} are set to be 18 ns and 14 ns, respectively, achieving a spatial resolution of 3.3 m according to Eq. (4). Meanwhile, τ_{pL} and τ_{wL} are optimized to be 120 ns and 94 ns, considering the influence of intensity fluctuation explained above. The odd and even pulses in the pair are separated by 40 μs. Here, only the SP method with 120 ns pulse is used as a reference since the spectrum of the SP-18ns would be too wide to estimate the wind profiles effectively. The peak power of both the SP-120ns and the DCP-18ns is limited to 250 W by the EDFA. The temporal resolution is set to 1 s, averaging over 12.5 k laser shots.

The backscattering power spectra from the DCP-18ns and the SP-120ns lidars are plotted in Fig. 5. For a more intuitive illustration, peak normalization is used. Similar to Figs. 4(c) and 4(d), the spectral width of the two schemes is quite close since the spectral width of the DCP method is mainly determined by the common pulse. Compared with Fig. 5(b), the spectrum in Fig. 5(a) reveals more details owing to the higher spatial resolution.

To observe the evolution of atmospheric wind field, continuous measurement over 4 s is carried out. The instruments are placed on the sixth floor of the Hefei National Laboratory building. As illustrated in Fig. 6, the wind velocity profiles measured by the two schemes show the same trend versus distance. Due to the influence of tall buildings on the campus, the wind field has a large gradient at some distances, for instance, the rapid change about 280 m away. The measurement results of the DCP-18ns varies continuously around the SP-120ns through time (like at 120 and 280 m). This continuity implies that the

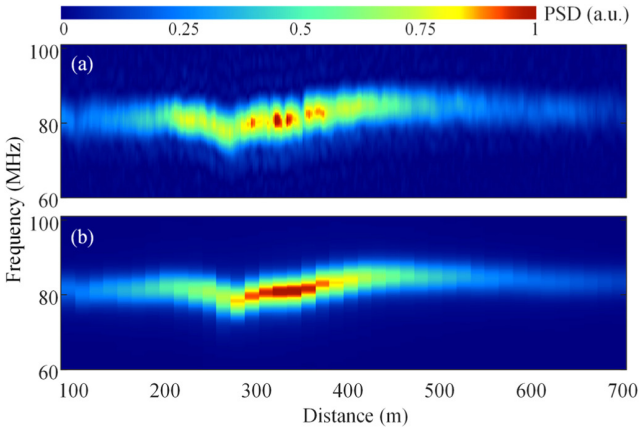

Fig. 5. Normalized backscattering power spectrum density measured by (a) DCP-18ns and (b) SP-120ns lidar with temporal resolution of 1 s.

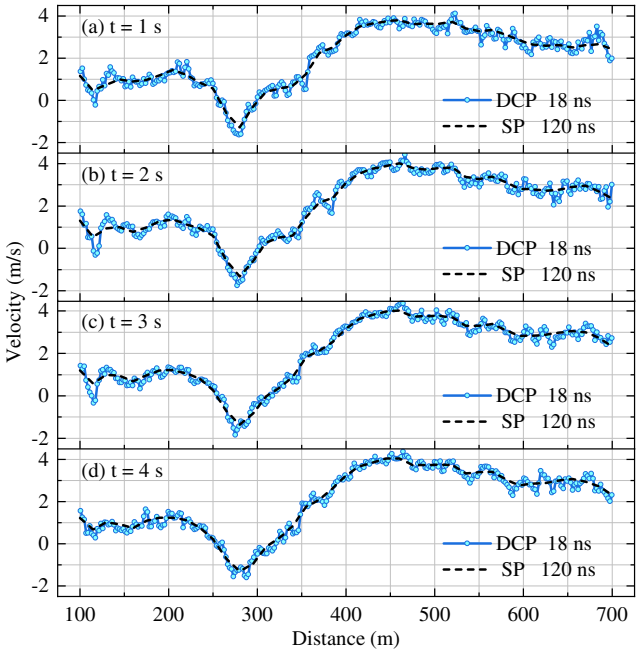

Fig. 6. Radial wind velocity profiles obtained by continuous observation over 4 s. (a)–(d) The DCP and the SP lidar measurements with temporal resolution of 1 s.

variation is more likely to be the time-varying characteristics of the fine wind field than the random measurement noise. Here, the accuracy of the radial wind estimation is set to be 0.1 m/s by data quality control of the CNR.

In conclusion, a CDWL utilizing differential correlation pair technique is demonstrated. The new scheme offers an approach to improve the spatial resolution and CNR without broadening the spectrum. Comparison experiments are carried out between the DCP CDWL and conventional CDWL, validating the performance of the proposed scheme. Under a specific spatial resolution, the duration of the common pulse needs to be further optimized, considering a trade-off between spectral width and optical stability. Since narrow linewidth lasers with a peak power higher than 1 kW have been realized [14], the performance such as detection distance of the proposed lidar could be promoted by upgrading the laser.

Funding. National Ten Thousand Talent Program in China; Strategic Priority Research Program of Chinese Academy of Sciences (XDA22040601).

Acknowledgment. We thank Mr. Manyi Li and Mr. Lijie Zhao for their help with the experiments.

Disclosures. The authors declare no conflicts of interest.

Data Availability. Data underlying the results presented in this Letter are not publicly available at this time but may be obtained from the authors upon reasonable request.

REFERENCES

1. B. Witschas, S. Rahm, A. Dörnbrack, J. Wagner, and M. Rapp, J. Atmos. Ocean. Technol. **34**, 1371 (2017).
2. M. Jia, J. Yuan, C. Wang, H. Xia, Y. Wu, L. Zhao, T. Wei, J. Wu, L. Wang, S.-Y. Gu, L. Liu, D. Lu, R. Chen, X. Xue, and X. Dou, Atmos. Chem. Phys. **19**, 15431 (2019).
3. Y. Yang, S. Fan, L. Wang, Z. Gao, Y. Zhang, H. Zou, S. Miao, Y. Li, M. Huang, S. H. L. Yim, and S. Lolli, Remote Sens. **12**, 3935 (2020).
4. N. J. Harvey, R. J. Hogan, and H. F. Dacre, Q. J. R. Meteorol. Soc. **141**, 1345 (2015).
5. C. Wang, M. Jia, H. Xia, Y. Wu, T. Wei, X. Shang, C. Yang, X. Xue, and X. Dou, Atmos. Meas. Tech. **12**, 3303 (2019).
6. Y. Yang, S. H. L. Yim, J. Haywood, M. Osborne, J. C. S. Chan, Z. Zeng, and J. C. H. Cheng, J. Geophys. Res. Atmos. **124**, 9609 (2019).
7. T. Mikkelsen, J. Phys. Conf. Ser. **524**, 012007 (2014).
8. T. Wei, H. Xia, B. Yue, Y. Wu, and Q. Liu, Opt. Express **29**, 17246 (2021).
9. J. Yuan, H. Xia, L. Wei, L. Wang, B. Yu, and Y. Wu, Opt. Express **28**, 37406 (2020).
10. I. N. Smalikho and V. A. Banakh, Opt. Lett. **40**, 3408 (2015).
11. S. Wu, X. Zhai, and B. Liu, Opt. Express **27**, 1142 (2019).
12. C. Wang, H. Xia, Y. Liu, S. Lin, and X. Dou, Opt. Commun. **424**, 48 (2018).
13. R. G. Frehlich and M. J. Kavaya, Appl. Opt. **30**, 5325 (1991).
14. F. Gustave, P. Bourdon, J. L. Gouët, A. Durécu, L. Lombard, H. Jacqmin, and A. Dolfi-Bouteyre, in *Conference on Lasers and Electro-Optics Europe & European Quantum Electronics Conference* (2019).
15. N. Prasad, R. Sibell, S. Vetorino, R. Higgins, and A. Tracy, Proc. SPIE **9465**, 94650C (2015).
16. C. Wang, H. Xia, Y. Wu, J. Dong, T. Wei, L. Wang, and X. Dou, Opt. Lett. **44**, 311 (2019).
17. R. Shibata, H. Kasahara, and T. Horiguchi, in *IEEE 6th International Conference on Photonics (ICP)* (2016).
18. M. S. D. Zan, Y. Masui, and T. Horiguchi, in *IEEE 7th International Conference on Photonics (ICP)* (2018).
19. T. Horiguchi, Y. Masui, and M. S. D. Zan, Sensors **19**, 1497 (2019).
20. P. Schroeder, W. A. Brewer, A. Choukulkar, A. Weickmann, M. Zucker, M. W. Holloway, and S. Sandberg, J. Atmos. Ocean. Technol. **37**, 1387 (2020).
21. V. Banakh and I. Smalikho, *Coherent Doppler Wind Lidars in a Turbulent Atmosphere* (Artech House, 2013).